Second-Order Sliding-Mode Controller Design and Its Implementation for Buck Converters

Shihong Ding, *Member, IEEE*, Wei Xing Zheng, *Fellow, IEEE*, Jinlin Sun, and Jiadian Wang

***Abstract*—A second-order sliding-mode (SOSM) control method is developed for the regulation problem of a dc–dc buck converter. By taking into account the model uncertainties and external disturbances in the mathematical model, a sliding variable with relative of degree 2 is first constructed. Then, a new SOSM controller is developed such that the output voltage will well track the desired reference voltage. Theoretical analysis shows that the resulting closed-loop system is globally finite-time stable, while similar SOSM control results only give the proof for finite-time convergence. The way on how to implement the proposed SOSM algorithm is also presented. The theoretical findings are verified by extensive simulations and experiments.**

***Index Terms*—Buck converter, finite-time control, Lyapunov stability, second-order sliding mode (SOSM).**

I. Introduction

SWITCHED-MODE dc–dc converters are power electronic devices employed to adapt the voltage and current levels between sources and loads, while maintaining a low power loss in the conversion process [1]. Buck converters are one of the most important switched-mode dc–dc converters, which have been widely used in various applications, such as photovoltaic systems, dc supply systems, etc. Basically, the control strategies play an important role for a buck converter because maintaining a tight regulation of the output voltage in the presence of disturbance is the ultimate goal.

It can be observed from the literature that the control design problems for buck converters are mostly based on a linear average mathematical model, and thus, conventional PID controllers are widely applied. However, they may not provide a satisfactory control performance under some large-signal operating conditions. Under this situation, the effect of lumped disturbances, which comes from the buck converters' uncertainties and external disturbances, could not be eliminated by the conventional PID controllers. To this end, various nonlinear control strategies have been utilized to control buck converters, for example, adaptive control [2], artificial neural network control [3], backstepping control [4], hierarchical control [5], etc. Among these nonlinear control strategies, the sliding-mode control (SMC) strategy has been paid much attention [6].

The SMC for buck converters has gained significant attention in recent years, and a number of research works have been reported, such as [7]–[9]. The general design issues of sliding-mode controllers for buck converters are introduced in [10]. Later, a simple and efficient approach for choosing a sliding-mode coefficient is given in [8] to ensure that the designed controller is also optimal. Meanwhile, a terminal sliding-mode (TSM) controller is developed in [11]. Unfortunately, there may be a singular problem in [11]. To tackle the singular problem, the nonsingular TSM controllers are designed in [7] and [12].

It should be pointed out that all the SMC controllers derived above are the conventional first-order SMC results. This implies that the performances of the closed-loop system are determined by the choice of the sliding-mode manifolds [13], [14]. However, it is known that it is not easy to design a proper sliding-mode manifold for catering the design requirements [15]. Different from the aforementioned first-order SMC methods, there are also some results for controlling buck converters using the second-order sliding mode (SOSM) control methods, such as [9]. However, it can be observed clearly from the literature that there are at least two problems for SOSM control of buck converters. One problem is that the existing results on SOSM control of buck converters are mostly based on geometric methods [9], [16], [17]. Under geometric methods, a direct evaluation of the explicit relations between the design parameters and steady-state errors in the presence of various perturbations is almost impossible. Meanwhile, only finite-time convergence can be guaranteed for the existing results. The other problem is that most of the SOSM methods for controlling buck converters only provide the simulation results, and few of them could give the implementation.

To resolve the aforementioned two open and yet important problems, a Lyapunov-based SOSM controller will be designed and implemented to show the advantages of a new kind of

Manuscript received July 16, 2017; revised September 9, 2017; accepted September 25, 2017. Date of publication September 29, 2017; date of current version May 2, 2018. This work was supported in part by the National Natural Science Foundation of China under Grant 61573170 and Grant 31571571, the Priority Academic Program Development of Jiangsu Higher Education Institutions, the Six Talent Peaks Project in Jiangsu Province under Grant XNYQC-006, and the Australian Research Council under Grant DP120104986. Paper no. TII-17-1571. *(Corresponding author: Wei Xing Zheng.)*

S. Ding and J. Wang are with the School of Electrical and Information Engineering, Jiangsu University, Zhenjiang 212013, China (e-mail: dsh@mail.ujs.edu.cn; wangjiadian1990@163.com).

W. X. Zheng is with the School of Computing, Engineering and Mathematics, Western Sydney University, Sydney, NSW 2751, Australia (e-mail: w.zheng@westernsydney.edu.au).

J. Sun is with the Institute of Automation, Chinese Academy of Sciences, Beijing 100190, China, and also with the University of Chinese Academy of Sciences, Beijing 100049, China (e-mail: jinlinsun@outlook.com).

Color versions of one or more of the figures in this paper are available online at http://ieeexplore.ieee.org.

Digital Object Identifier 10.1109/TII.2017.2758263

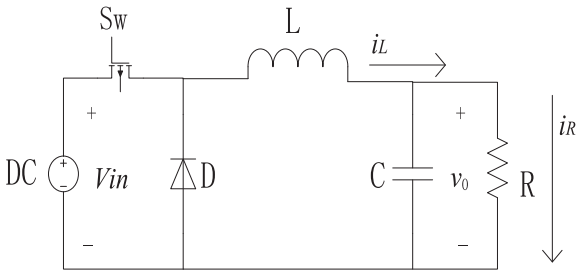

Fig. 1. Circuit diagram of the buck converter.

SOSM controller in this paper. First of all, taking the external disturbances and uncertainties into account, a practical model is developed by making full use of the average model of buck converters. Based on the practical model, a sliding variable with relative of degree 2 is constructed, which assures that the stabilization of the sliding variable implies the solvability of the regulation problem. Second, by applying the modified version of the adding a power integrator technique [18], [19], the SOSM controller can be constructed recursively by means of a step-by-step design procedure. Under the developed SOSM controller, it can be proved that the closed-loop system of the buck converter is finite-time Lyapunov stable rather than only finite-time convergent. Third, the implementation issue of the proposed SOSM algorithm is discussed, and a hysteresis-based implementation strategy is developed. Finally, simulation and experiment results are given to illustrate the effectiveness of the proposed method.

The contributions of this paper can be briefly summarized as two aspects. One contribution is that the used fundamental theory is different from the existing results. It can be clearly observed that the existing SOSM controllers in dc–dc buck converters are based on supertwisting or suboptimal algorithms. In contrast, the SOSM controller given here is based on the Lyapunov method, and the evaluation of the explicit relations between the design parameters and steady-state errors may be derived. The second contribution is that the finite-time stability of the closed-loop buck converter system can be obtained. Note that all sliding variables of the buck converter systems considered in the literature are finite-time convergent but not finite-time stable. The finite-time stability is much stronger than the finite-time convergence because the former includes the latter plus Lyapunov stability.

II. Modeling the Buck Converter

Generally, a buck converter consists of a dc voltage source ($V_{\rm in}$), a controllable switch (Sw), a diode (D), an inductor (L), a capacitor (C), and a load resistor (R), properly connected as depicted in Fig. 1.

Assume that the parameters of the buck converter are known and the disturbances are absent. By using the state-space averaging method, the ideal average model can be described as the following two cases. When the switch Sw is turned ON, the operation of buck converter can be described as

$$\frac{di_L}{dt} = \frac{1}{L}(V_{\rm in} - v_0), \quad \frac{dv_0}{dt} = \frac{1}{C}\left(i_L - \frac{v_0}{R}\right). \tag{1}$$

When the switch Sw is turned OFF, the operation of buck converter can be described as

$$\frac{di_L}{dt} = -\frac{v_0}{L}, \quad \frac{dv_0}{dt} = \frac{1}{C}\left(i_L - \frac{v_0}{R}\right). \tag{2}$$

Combining (1) and (2), the average model is as follows [20]:

$$\frac{di_L}{dt} = \frac{1}{L}(\mu V_{\rm in} - v_0), \quad \frac{dv_0}{dt} = \frac{1}{C}\left(i_L - \frac{v_0}{R}\right)$$

where μ is the switch, which takes "1" and "0" for the switch states ON and OFF, respectively. The switch μ is determined by a control scheme U, which will be designed later.

As a matter of fact, there are uncertainties and external disturbances existing in the average mode. To model the buck converter accurately, a practical model can be considered as

$$\begin{aligned}\frac{di_L}{dt} &= \frac{1}{L_0 + \Delta L}(\mu(V_{\rm in0} + \Delta V_{\rm in}) - v_0) + d_1(t)\\ \frac{dv_0}{dt} &= \frac{1}{C_0 + \Delta C}\left(i_L - \frac{v_0}{R_0 + \Delta R}\right) + d_2(t)\end{aligned} \tag{3}$$

where L_0, C_0, R_0, and $V_{\rm in0}$ are the nominal parts of L, C, R, and $V_{\rm in}$, and $\Delta L, \Delta C, \Delta R$, and $\Delta V_{\rm in}$ are variations of L, C, R, and $V_{\rm in}$, respectively. $d_1(t)$ and $d_2(t)$ are the unknown bounded disturbances, such as unmodeled dynamics, load perturbations, electromagnetic interference, etc. It is assumed that the first-order derivatives of $d_1(t)$ and $d_2(t)$ are bounded. By a simple calculation, system (3) can be rewritten as

$$\begin{aligned}\frac{di_L}{dt} &= \frac{1}{L_0}(\mu V_{\rm in0} - v_0) + w_1(t)\\ \frac{dv_0}{dt} &= \frac{1}{C_0}\left(i_L - \frac{v_0}{R_0}\right) + w_2(t)\end{aligned} \tag{4}$$

where the lumped disturbances $w_1(t)$ and $w_2(t)$ are given by

$$\begin{aligned}w_1(t) &= \frac{\mu\Delta V_{\rm in} L_0 - \mu\Delta L V_{\rm in0} + \Delta L v_0}{(L_0 + \Delta L)L_0} + d_1(t)\\ w_2(t) &= \frac{v_0\Delta R}{R_0(R_0 + \Delta R)(C_0 + \Delta C)} + \frac{v_0\Delta C - i_L\Delta C R_0}{C_0 R_0(C_0 + \Delta C)}\\ &\quad + d_2(t).\end{aligned}$$

The aim of this paper is to design a control strategy such that the output voltage v_0 will well track a desired reference voltage $v_{\rm ref}$ in the presence of the lumped disturbances $w_1(t)$ and $w_2(t)$.

At the end of this section, we list three lemmas that serve as the basis of the key tools for the subsequent controller design.

Lemma 1 (see [21]): If $p_1 > 0$ and $0 < p_2 \le 1$, then the following inequality holds:

$$|\lceil x\rfloor^{p_1 p_2} - \lceil y\rfloor^{p_1 p_2}| \le 2^{1-p_2}|\lceil x\rfloor^{p_1} - \lceil y\rfloor^{p_1}|^{p_2} \quad \forall x, y \in \mathbb{R}.$$

Lemma 2 (see [18]): Let c and d be positive constants. Given any positive function $\gamma > 0$, the following inequality holds:

$$|x|^c|y|^d \le \frac{c}{c+d}\gamma|x|^{c+d} + \frac{d}{c+d}\gamma^{-\frac{c}{d}}|y|^{c+d} \quad \forall x, y \in \mathbb{R}.$$

Lemma 3 (see [22]): Let p be a real number with $0 < p < 1$. Then, one has $(|x_1| + \cdots |x_n|)^p \le |x_1|^p + \cdots + |x_n|^p$, $\forall x_i \in \mathbb{R}, i = 1, \ldots, n$.

III. SOSM Controller Design

In this section, a Lyapunov-based SOSM control strategy will be presented for controlling the buck converter. There are two steps in the control design. In the first step, by using the modified version of the adding a power integrator technique [18], [19], an SOSM controller is first constructed step by step, and the rigorous mathematical analysis is also made. In the second step, the detailed way on how to implement the proposed SOSM algorithm is presented. Given below first are some backgrounds for SOSM.

A. Brief Description for SOSM

Consider the nonlinear dynamical system

$$\dot{x} = f(t,x) + g(t,x)U, \quad s = s(t,x)$$

where $x \in \mathbb{R}^n$ and $U \in \mathbb{R}$ are the system state and the control input, respectively, $f(t,x)$ and $g(t,x)$ are smooth functions, and $s \in \mathbb{R}$ is the output (sliding variable). The sliding variables s and $\dot{s} = ds/dt$ are assumed to be known. Supposing that the sliding variable s has a relative degree $r = 2$ with respect to controller U, one has

$$\ddot{s} = a(t,x) + b(t,x)U$$

where $a(t,x) = \ddot{s}|_{U=0}$ and $b(t,x) = \frac{\partial \ddot{s}}{\partial U}$ are not exactly known, but satisfy the following assumption.

Assumption 1: There exist three positive constants $\bar{a}, \underline{b}$, and $\bar{b}$ such that $|a(t,x)| \le \bar{a}$, $\underline{b} \le b(t,x) \le \bar{b}$.

According to [23], the sliding mode is called the SOSM if $s = \dot{s} = 0$ can be kept. The SOSM control of nonlinear systems has been widely studied recently, resulting in several algorithms which include the supertwisting algorithm [23], the suboptimal algorithm [24], etc. However, it can be clearly observed that the aforementioned well-known SOSM algorithms are based on geometric methods. Different from those methods, we are going to design a Lyapunov-based SOSM controller for the regulation problem of the buck converter. The designed controller will provide the finite-time Lyapunov stability for the resulting closed-loop system.

B. Controller Design

Based on the SOSM theory presented in Section III-A, to design an SOSM controller for system (4), the first thing to do is to choose a sliding variable. We now define the sliding variable s (i.e., the voltage error) as $s = v_0 - v_{\text{ref}}$, where v_{ref} denotes the dc reference output voltage. Note that the switch μ is determined by the control scheme U. By (4), we can obtain the dynamics of the sliding variable s directly as

$$\ddot{s} = a(t,x) + b(t,x)U \tag{5}$$

with $a(t,x) = (\frac{1}{(R_0C_0)^2} - \frac{1}{L_0C_0})v_0 - \frac{i_L}{R_0C_0^2} + \frac{w_1(t)}{C_0} - \frac{w_2(t)}{R_0C_0} + \dot{w}_2(t)$ and $b(t,x) = \frac{v_{\text{in}0}}{L_0C_0}$.

Let $v_0^{\max}$ and $i_L^{\max}$ be the maximum of v_0 and i_L, respectively. Then, by a simple calculation, we can obtain from Fig. 1 that the following estimation holds:

$$0 \le v_0 \le v_0^{\max} \le v_{\text{ref}} + \Delta_1, \quad 0 \le i_L \le i_L^{\max} \le \frac{v_{\text{ref}}}{R_0} + \Delta_2 \tag{6}$$

where Δ_1 and Δ_2 are small constants caused by perturbations. Let $\Delta = \max\{\Delta_1, \Delta_2\}$. By (6), we have

$$|a(t,x)| \le \left|\frac{1}{(R_0C_0)^2} - \frac{1}{L_0C_0}\right|(v_{\text{ref}} + \Delta) + \frac{v_{\text{ref}} + R_0\Delta}{R_0^2C_0^2} + \left|\frac{w_1(t)}{C_0} - \frac{w_2(t)}{R_0C_0} + \dot{w}_2(t)\right|. \tag{7}$$

In view of the definition of the lumped disturbances w_1 and w_2, there exists a constant $d > 0$ such that

$$\left|\frac{1}{(R_0C_0)^2} - \frac{1}{L_0C_0}\right|\Delta + \frac{\Delta}{R_0C_0^2} + \left|\frac{w_1(t)}{C_0} - \frac{w_2(t)}{R_0C_0} + \dot{w}_2(t)\right| \le d.$$

Then, it follows from (7) that

$$|a(t,x)| \le \left|\frac{1}{(R_0C_0)^2} - \frac{1}{L_0C_0}\right|v_{\text{ref}} + \frac{v_{\text{ref}}}{R_0^2C_0^2} + d. \tag{8}$$

Let L_0, C_0, R_0, and a positive constant β_1 be chosen such that the following condition holds:

$$\frac{V_{\text{in}0}}{L_0C_0} > \left|\frac{1}{(R_0C_0)^2} - \frac{1}{L_0C_0}\right|v_{\text{ref}} + \frac{v_{\text{ref}}}{R_0^2C_0^2} + d + \frac{27}{\beta_1^{3/2}} + 2^{1/2}\beta_1 + \beta_1^{11/6} + \frac{1}{4}\beta_1^{1/2}. \tag{9}$$

The task here is now to design an SOSM controller U under condition (9) such that the output voltage v_0 will track the reference voltage v_{ref}.

To simplify the expression, we first denote $\lceil x \rfloor^\alpha = |x|^\alpha \operatorname{sign}(x)$. For system (5), the SOSM controller is constructed as

$$U = -\operatorname{sign}(\lceil \dot{s} \rfloor^2 + \beta_1 s) \tag{10}$$

with a properly chosen positive constant β_1.

Remark 1: It will be seen from the proof of Theorem 1 that inequality (9) is a precondition to guarantee the finite-time stability of the closed-loop system (5), (10). However, by (9), it seems that the choice of the parameter β_1 is conservative. In fact, we employ a backstepping-like method to deal with the control design. Due to the nature of the backstepping method, the terms about β_1 in condition (9) are brought about during the backstepping design. Fortunately, we could give some guidelines on how to choose the parameter β_1 in this paper although it seems to be conservative. Specifically, by a simple calculation, we make sure that $\frac{V_{\text{in}0}}{L_0C_0} > |\frac{1}{(R_0C_0)^2} - \frac{1}{L_0C_0}|v_{\text{ref}} + \frac{v_{\text{ref}}}{R_0^2C_0^2}$. Then, the parameter β_1 can be tuned from $(0, \frac{V_{\text{in}0}}{L_0C_0} - |\frac{1}{(R_0C_0)^2} + \frac{1}{L_0C_0}|v_{\text{ref}} - \frac{v_{\text{ref}}}{R_0^2C_0^2})$, until the best performance of the closed-loop system can be reached.

Now, we have the following result.

Theorem 1: Considering the SOSM dynamics (5), controller (10) provides for the finite-time establishment of SOSM $s = \dot{s} = 0$, in the sense that, under controller (10), the output voltage v_0 will track the reference voltage v_{ref} in a finite time.

Proof: Let $y_1 = s,\ y_2 = \dot{s}$. System (5) and controller (10) can be rewritten as

$$\dot{y}_1 = y_2,\ \ \dot{y}_2 = a(t,x) + b(t,x)U \tag{11}$$

$$U = -\operatorname{sign}(\lceil y_2 \rfloor^2 + \beta_1 y_1) \tag{12}$$

respectively. In the following, we will prove the finite-time stability of the closed-loop system (11) and (12) using the adding a power integrator method proposed in [18] and [19]. The proof will be carried out by two steps. First, a virtual controller y_1^* will be constructed such that y_1 will be stabilized to zero. Second, the real controller U will be developed to make sure that the state y_2 will finite-time track y_2^*.

Step 1: We choose the Lyapunov function $V_1(y_1) = \frac{2|y_1|^{5/2}}{5}$. Taking the derivative of $V_1(y_1)$ produces

$$\dot{V}_1(y_1) = \lceil y_1 \rfloor^{3/2} y_2 = \lceil y_1 \rfloor^{3/2} y_2^* + \lceil y_1 \rfloor^{3/2}(y_2 - y_2^*)$$

where y_2^* is a virtual control law. Designing y_2^* as $y_2^* = -\beta_1^{1/2}\lceil y_1 \rfloor^{1/2},\ \beta_1 > 0$ yields

$$\begin{aligned}\dot{V}_1(y_1) &= \lceil y_1 \rfloor^{3/2} y_2^* + \lceil y_1 \rfloor^{3/2}(y_2 - y_2^*) \\ &= -\beta_1^{1/2}\lceil y_1 \rfloor^{3/2}\lceil y_1 \rfloor^{1/2} + \lceil y_1 \rfloor^{3/2}(y_2 - y_2^*) \\ &= -\beta_1^{1/2} y_1^2 + \lceil y_1 \rfloor^{3/2}(y_2 - y_2^*).\end{aligned} \tag{13}$$

Step 2: Choose a function as

$$V_2(y_1, y_2) = V_1(y_1) + W(y_1, y_2)$$

with $W(y_1, y_2) = \int_{y_2^*}^{y_2} \lceil \lceil \kappa \rfloor^2 - \lceil y_2^* \rfloor^2 \rfloor^2 d\kappa$. It can be easily verified that the function $V_2(y_1, y_2)$ is C^1, positive definite, and proper. From (13), the following estimate holds:

$$\begin{aligned}\dot{V}_2(y_1, y_2) \le\ & -\beta_1^{1/2} y_1^2 + \lceil y_1 \rfloor^{3/2}(y_2 - y_2^*) \\ & + \frac{\partial W(y_1, y_2)}{\partial y_1}\dot{y}_1 + \lceil \xi \rfloor^2 \dot{y}_2\end{aligned} \tag{14}$$

with $\xi = \lceil y_2 \rfloor^2 - \lceil y_2^* \rfloor^2$. Next, we estimate each term in the right-hand side of (14).

According to Lemma 1, we can obtain

$$\begin{aligned}\lceil y_1 \rfloor^{3/2}(y_2 - y_2^*) &\le |y_1|^{3/2}\left|\lceil y_2 \rfloor^{2\times\frac{1}{2}} - \lceil y_2^* \rfloor^{2\times\frac{1}{2}}\right| \\ &\le 2^{1/2}|y_1|^{3/2}|\xi|^{1/2}.\end{aligned} \tag{15}$$

Meanwhile, using Lemma 2, we have

$$2^{1/2}|y_1|^{3/2}|\xi|^{1/2} \le 2^{1/2} \times \frac{3}{4}\gamma y_1^2 + 2^{1/2} \times \frac{1}{4}\gamma^{-3}\xi^2. \tag{16}$$

Letting $2^{1/2} \times \frac{3}{4}\gamma = \frac{\beta_1^{1/2}}{4}$, one has $\gamma = \frac{\beta_1^{1/2}}{3\times 2^{1/2}}$. By (15) and (16), the following estimate holds:

$$\lceil y_1 \rfloor^{3/2}(y_2 - y_2^*) \le \frac{\beta_1^{1/2}}{4} y_1^2 + \left(\frac{3}{\beta_1^{1/2}}\right)^3 \xi^2. \tag{17}$$

Noting that $\frac{\partial \lceil y_2^* \rfloor^2}{\partial y_1} = -\beta_1$, it can be concluded from Lemma 1 that

$$\begin{aligned}\frac{\partial W(y_1, y_2)}{\partial y_1}\dot{y}_1 &\le \left|\lceil y_2 \rfloor^{2\times\frac{1}{2}} - \lceil y_2^* \rfloor^{2\times\frac{1}{2}}\right||\xi|\left|\frac{\partial \lceil y_2^* \rfloor^2}{\partial y_1} y_2\right| \\ &\le 2^{1/2}\beta_1|\xi|^{3/2}|y_2|.\end{aligned} \tag{18}$$

Since $|y_2| = |\lceil y_2 \rfloor^2|^{1/2} = |\xi + \lceil y_2^* \rfloor^2|^{1/2} \le (|\xi| + |y_2^*|^2)^{1/2}$, it follows from Lemma 3 that $|y_2| \le |\xi|^{1/2} + |y_2^*|$. Consequently, (18) can be rewritten as

$$\begin{aligned}\frac{\partial W(y_1, y_2)}{\partial y_1}\dot{y}_1 &\le 2^{1/2}\beta_1|\xi|^{3/2}(|\xi|^{1/2} + |y_2^*|) \\ &\le 2^{1/2}\beta_1\xi^2 + 2^{1/2}\beta_1^{3/2}|\xi|^{3/2}|y_1|^{1/2}.\end{aligned} \tag{19}$$

Using Lemma 2 again, one has

$$\begin{aligned}&2^{1/2}\beta_1^{3/2}|\xi|^{3/2}|y_1|^{1/2} \\ &\le 2^{1/2}\beta_1^{3/2} \times \frac{1}{4}\gamma y_1^2 + 2^{1/2}\beta_1^{3/2} \times \frac{3}{4} \times \gamma^{-1/3}\xi^2.\end{aligned} \tag{20}$$

Letting $2^{1/2}\beta_1^{3/2} \times \frac{1}{4}\gamma = \frac{1}{2}\beta_1^{1/2}$ yields $\gamma = \frac{2^{1/2}}{\beta_1}$. By (20) and a simple calculation, it is clear that

$$2^{1/2}\beta_1^{3/2}|\xi|^{3/2}|y_1|^{1/2} \le \frac{1}{2}\beta_1^{1/2} y_1^2 + \beta_1^{11/6}\xi^2. \tag{21}$$

Substituting (21) into (19) gives

$$\frac{\partial W(y_1, y_2)}{\partial y_1}\dot{y}_1 \le \frac{1}{2}\beta_1^{1/2} y_1^2 + \left(2^{1/2}\beta_1 + \beta_1^{11/6}\right)\xi^2. \tag{22}$$

Combining (17) and (22) together, it can be concluded from (14) that

$$\begin{aligned}\dot{V}_2(y_1, y_2) \le\ & \left(\frac{27}{\beta_1^{3/2}} + 2^{1/2}\beta_1 + \beta_1^{11/6}\right)\xi^2 \\ & - \frac{\beta_1^{1/2}}{4} y_1^2 + \lceil \xi \rfloor^2(a(t,x) + b(t,x)U).\end{aligned} \tag{23}$$

With the fact $\lceil y_2 \rfloor^2 - \lceil y_2^* \rfloor^2 = \lceil y_2 \rfloor^2 + \beta_1 y_1 = \xi$ and $b(t,x) = \frac{V_{\text{in}0}}{L_0 C_0}$ in mind, substituting (12) into (23) yields

$$\begin{aligned}\dot{V}_2(y_1, y_2) \le\ & -\frac{\beta_1^{1/2}}{4} y_1^2 + \left(\frac{27}{\beta_1^{3/2}} + 2^{1/2}\beta_1 + \beta_1^{11/6}\right)\xi^2 \\ & + \xi^2|a(t,x)| - b(t,x)\lceil \xi \rfloor^2 \cdot \operatorname{sign}(\xi) \\ \le\ & -\frac{\beta_1^{1/2}}{4} y_1^2 + \left(\frac{27}{\beta_1^{3/2}} + 2^{1/2}\beta_1 + \beta_1^{11/6}\right)\xi^2 \\ & + \xi^2|a(t,x)| - \xi^2\frac{V_{\text{in}0}}{L_0 C_0}.\end{aligned}$$

From (8), we have $|a(t,x)| \le \left|\frac{1}{(R_0 C_0)^2} - \frac{1}{L_0 C_0}\right| v_{\text{ref}} + \frac{v_{\text{ref}}}{R_0^2 C_0^2} + d$. In addition, by condition (9), we know

$$\begin{aligned}\frac{V_{\text{in}0}}{L_0 C_0} >\ & \left|\frac{1}{(R_0 C_0)^2} - \frac{1}{L_0 C_0}\right| v_{\text{ref}} + \frac{v_{\text{ref}}}{R_0^2 C_0^2} + d \\ & + \frac{27}{\beta_1^{3/2}} + 2^{1/2}\beta_1 + \beta_1^{11/6} + \frac{1}{4}\beta_1^{1/2}.\end{aligned}$$

This implies $\dot{V}_2(y_1, y_2) \leq -\frac{\beta_1^{1/2}}{4}(y_1^2 + \xi^2)$. By the fact

$$\int_{y_2^*}^{y_2} \lceil \lceil \kappa \rfloor^2 - \lceil y_2^* \rfloor^2 \rfloor^2 d\kappa \leq |y_2 - y_2^*||\xi|^2 \leq 2^{\frac{1}{2}}|\xi|^{\frac{5}{2}}$$

we obtain

$$V_2(y_1, y_2) \leq 2(|y_1|^{\frac{5}{2}} + |\xi|^{\frac{5}{2}}). \tag{24}$$

Letting $c = 2^{-\frac{14}{5}}\beta_1^{1/2}$, $\alpha = \frac{4}{5}$, and using Lemma 3 and (24), we arrive at $\dot{V}_2(y_1, y_2) + cV_2^{\alpha}(y_1, y_2) \leq 0$. Note that $0 < \alpha < 1$. From the finite-time Lyapunov theory given in [25], it follows that system (11) can be globally finite-time stabilized by controller (12). ■

Remark 2: It should be pointed out that several SOSM algorithms for dc–dc buck converters have already been reported in the literature, such as [9], [16], and [17]. However, the result proposed in this paper is different from the existing results in two aspects. The first difference is that the basic theory used for the SOSM controller design is different. It can be clearly observed that the SOSM controllers in [9] are based on the supertwisting algorithm and the SOSM controllers in [16] and [17] are all based on the suboptimal algorithm, while the SOSM controller in this paper is built upon the Lyapunov method. The advantage of Lyapunov analysis lies in that a direct evaluation of the explicit relations between the design parameters and steady-state errors in the presence of various perturbations may be possible [26]. The second difference is that the finite-time stability of sliding variables can be obtained in this paper, while similar results can only give the finite-time convergence. It is noticed that all the sliding variables of the systems considered in [9], [16], and [17] are finite-time convergent rather than finite-time stable. Finite-time stability covers finite-time convergence plus Lyapunov stability. This implies that from the theoretical viewpoint, the existing SOSM algorithms may be unstable.

C. Realization of the SOSM Controller

By (10), we know that the SOSM controller includes two modes: $U = 1$ or $U = -1$. It is obvious that the switch μ can be determined by the following relation [20]:

$$\mu = \frac{1}{2}(1 + \text{sign}(U)). \tag{25}$$

On the other hand, it can be clearly seen from (10) that the sign function will lead to an infinite switching frequency when the sliding variables reach $\lceil \dot{s} \rfloor^2 + \beta_1 s = 0$. This implies that a direct implementation of controller (10) for the buck converter is not applicable because the switching frequency is too high. However, the operation frequency can be restricted within a tunable range, although it is not possible to determine how wide the range is. Similar to [27], this can be accomplished using a hysteresis modulation. In this paper, we redesign (25) as

$$\mu = \begin{cases} 1, & \text{when } \lceil \dot{s} \rfloor^2 + \beta_1 s < -\lambda \\ 0, & \text{when } \lceil \dot{s} \rfloor^2 + \beta_1 s > \lambda \\ \text{unchanged}, & \text{otherwise} \end{cases} \tag{26}$$

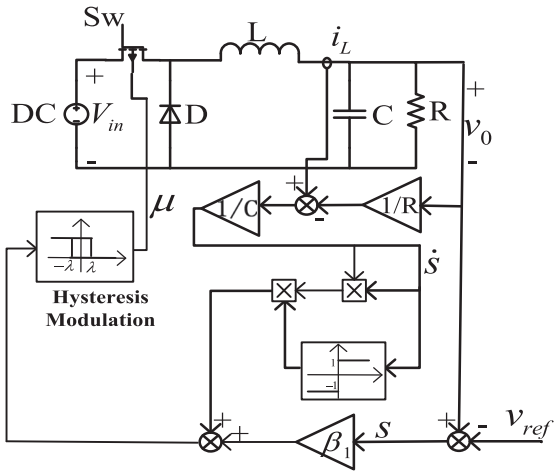

Fig. 2. Block diagram of a control scheme for the buck converter.

where λ is a small number, which provides the region given by

$$\Omega = \{-\lambda < \lceil \dot{s} \rfloor^2 + \beta_1 s < \lambda\}.$$

With this modification, the switching operation will not occur in the region Ω. Consequently, such modification can be employed to alleviate the infinite switching frequency in SOSM control. As a matter of fact, the output voltage error will converge to the region $|\lceil \dot{s} \rfloor^2 + \beta_1 s| < \lambda$, which shows that the larger λ implies the lower switching frequency and the smaller λ implies the higher switching frequency. This is because for a larger λ, the sliding variables can stay in the region $|\lceil \dot{s} \rfloor^2 + \beta_1 s| < \lambda$ for a longer time, while for a smaller λ, the sliding variables will stay in the region $|\lceil \dot{s} \rfloor^2 + \beta_1 s| < \lambda$ for a shorter time. On the other hand, it is difficult to actually give an explicit formula to calculate the parameter λ. The selection of λ is dependent on our experiences and a basic rule is the smaller the better. However, in reality, we have found that when λ is tuned to be a certain small level, the performance of the buck converter may be unchanged, even if the value of λ is further decreased. This may be caused by hardware constraint.

Under this modification, the control scheme can be illustrated as in Fig. 2.

Remark 3: Note that the sliding variables will converge to the region $|\lceil \dot{s} \rfloor^2 + \beta_1 s| < \lambda$. It can be easily obtained that $\dot{s}|\dot{s}| < \lambda - \beta_1 s$. Let $V(s) = \frac{1}{2}s^2$. By a simple calculation, we have $\dot{V}(s) \leq \frac{-\beta_1 s^2 + \lambda|s|}{|\dot{s}|}$, which implies that the sliding variables will converge to the region $\{s : |s| \leq \frac{\lambda}{\beta_1}\}$.

Remark 4: Though SOSM has some advantages, for example, simple structure and accuracy improvement, some inherited shortcomings remain to exist, such as the requirements of successive total time derivatives of sliding variables, the loss of order reduction property in applications, etc. These drawbacks may affect the robustness and anti-interference performance of the closed-loop system [28]. Fortunately, the mathematical model of buck converters is comparatively accurate, and the relative degree of the closed-loop system is low. These properties guarantee that the proposed method can provide a satisfactory control performance for the buck converter system.

TABLE I
COMPONENTS VALUES OF THE BUCK CONVERTER

Input Voltage ($V_{\rm in}$)	30 V
Inductance (L)	330 μH
Capacitance (C)	1000 μF
Load resistance (R)	100 Ω
Reference output voltage ($v_{\rm ref}$)	15 V

IV. SIMULATION AND EXPERIMENTAL RESULTS

In order to demonstrate the performance of the proposed SOSM algorithm, the closed-loop buck converter system under controller (26) is now tested by simulations and experiments. The specifications of the buck converter are given in Table I. For simulation, the lumped disturbances are set as $w_1(t) = 0.1\sin(2t)$ and $w_2(t) = 0.1\cos(2t)$. The constant β_1 is chosen as $1, 5$, and 10. Meanwhile, λ is also selected as $1, 5,$ and 10. By a simple calculation, we can verify that condition (9) holds.

Based on the parameters and conditions chosen above, the simulations and experiments will be conducted by using MATLAB software and DSP-based experiment platform, respectively. First of all, the comparisons under SOSM, first-order sliding mode (FOSM) and PID will be given. By taking the sliding-mode surface as $S = \dot{s} + c_1 s$ with $\forall c_1 > 0$, the FOSM controller can be designed as

$$u = -\frac{L_0C_0}{V_{\rm in0}}\left[\left(\frac{1}{R_0^2C_0^2} - \frac{1}{L_0C_0} - \frac{c_1}{R_0C_0}\right)v_0 + \left(\frac{c_1}{C_0} - \frac{1}{R_0C_0^2}\right)i_L + \eta\cdot\text{sign}(S)\right] \quad (27)$$

with $\eta > 0$. Meanwhile, according to the linear control theory, one can easily design the PID controller for the buck converter system as

$$u_{\rm PID} = K_p * s + K_i * \int sdt + K_d * \dot{s}. \quad (28)$$

Then, we want to verify the performance of the closed-loop system under SOSM controller (26) with different β_1. Finally, we will examine the influence of λ.

To try to make a fair comparison, the control input is restricted to be 5 V, and the parameters of the PID controller (28) and the FOSM controller (27) will be tuned to guarantee a good tradeoff among tracking and disturbance rejection performances.

A. Numerical Simulations

The sampling time is taken as 1 ms, and the initial state is selected as $(i_L(0), v(0)) = (0, 0)$. The signum function in FOSM is replaced by a hysteresis modulation with $\lambda = 1$ (hysteresis width). To obtain the best performance, the parameters of the PID controller (28) and the FOSM controller (27) are taken as $K_p = 13, K_i = 5.5, K_d = 0.01,$ and $c_1 = 2, \eta = 4\times10^5$, respectively. During the simulation, we assume that the load decreases to 50 Ω at time $t = 4$ s and then rises to 100 Ω at time $t = 6$ s.

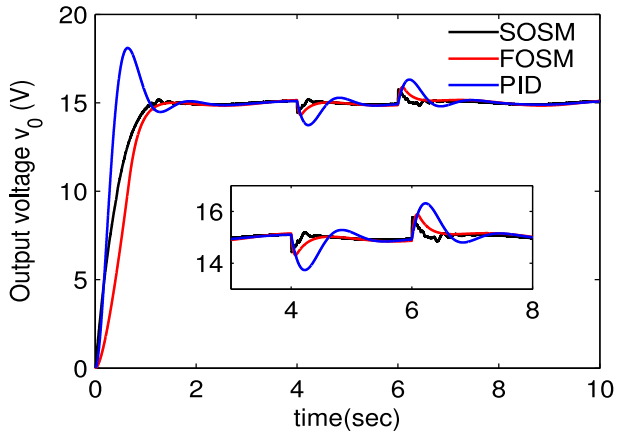

Fig. 3. Simulated start-up transient results of output voltage v_0 under the PID controller (28), the FOSM controller (27), and the SOSM controller (26) with $\lambda = 1, \beta_1 = 10$.

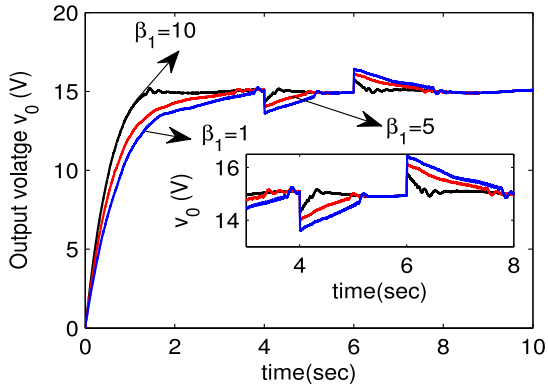

Fig. 4. Simulated step-load transient results of the output voltage under the SOSM controller (26) with $\lambda = 1$ and different β_1.

We first compare the control performance among the proposed SOSM controller, the conventional FOSM controller, and the traditional PID controller. The simulation results are shown in Fig. 3, from which it can be clearly seen that SOSM (26) possesses the best performance. In fact, the start-up performance for the FOSM controller (27) and the PID controller (28) can be improved a bit by tuning the parameters, but the disturbance rejection will get worse. From the disturbance rejection point of view, no matter how to tune the parameters, the SOSM controller will possess the best performance and the PID controller will exhibit the worst performance.

We then verify how the parameter β_1 can affect the convergence of the closed-loop system under the lumped disturbances. The corresponding simulation results are displayed in Figs. 4 and 5 that show the response curves of the output voltage and the sliding variable s under controller (26) with $\lambda = 1$ and different β_1, respectively. From Fig. 5, it can be clearly observed that with the increase of β_1, the convergence rate of the sliding variable s increases, too. Moreover, we also examine how β_1 can affect the output voltage when the input voltage changes. The simulation is done under the assumption that the input voltage decreases

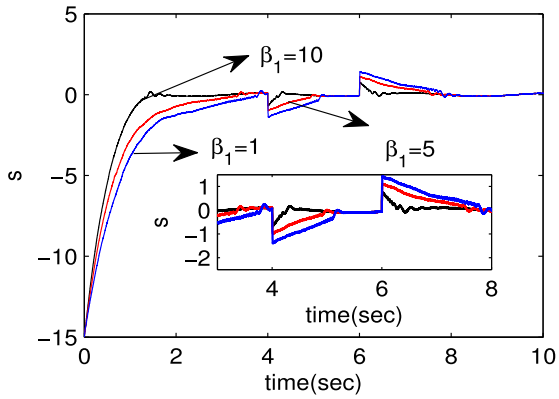

Fig. 5. Simulated step-load transient results of the sliding variable s under the SOSM controller (26) with $\lambda = 1$ and different β_1.

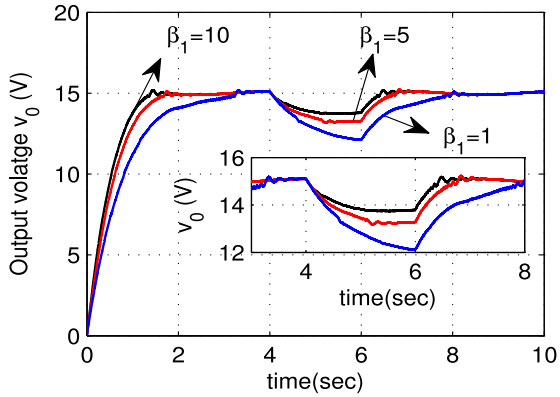

Fig. 6. Simulated step-input-voltage transient results of the output voltage under the SOSM controller (26) with $\lambda = 1$ and different β_1.

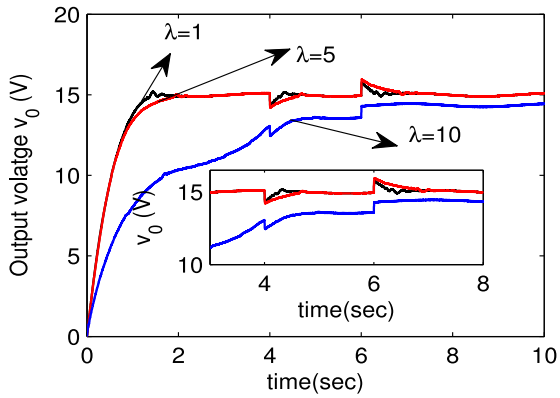

Fig. 7. Simulated step-load transient results of the output voltage under the SOSM controller (26) with $\beta_1 = 10$ and different λ.

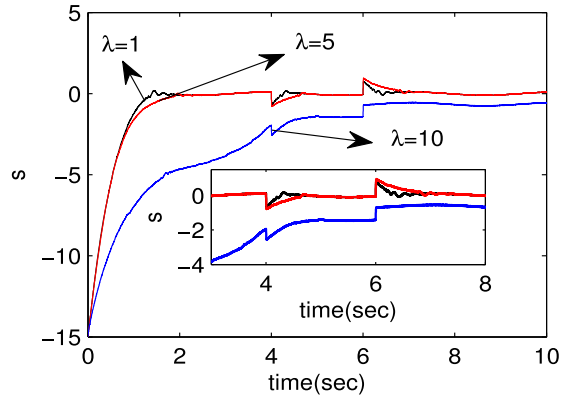

Fig. 8. Simulated step-load transient results of the sliding variable s under the SOSM controller (26) with $\beta_1 = 10$ and different λ.

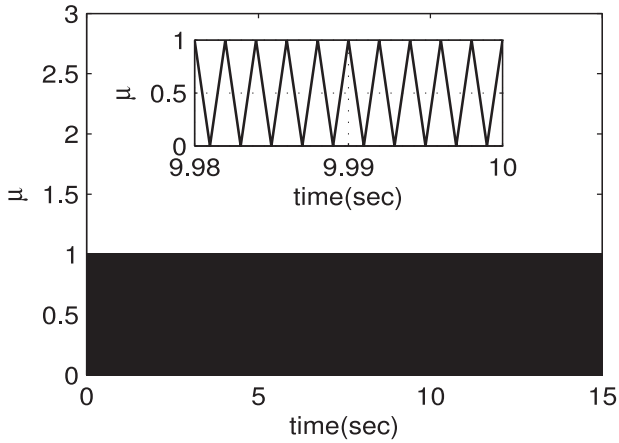

Fig. 9. Response curve of the control signal μ under $\beta_1 = 10, \lambda = 1$.

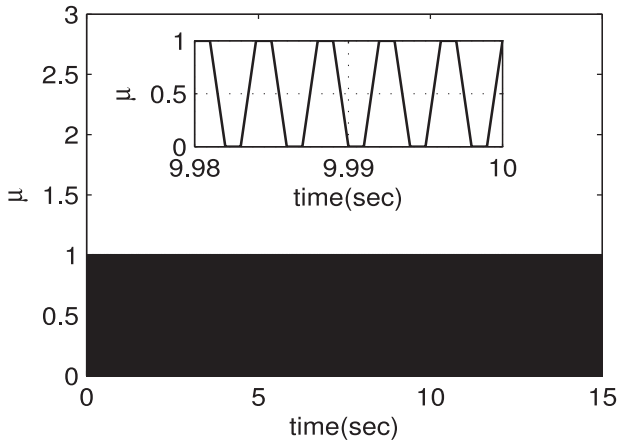

Fig. 10. Response curve of the control signal μ under $\beta_1 = 10, \lambda = 5$.

to 20 V at time $t = 4$ s and then rises to 30 V at time $t = 6$ s. Fig. 6 shows the performance comparisons when the input voltage varies. From Fig. 6, one can clearly see that the larger β_1 provides the better disturbance rejection property. These simulation results tell that the increase of β_1 implies both the better disturbance rejection property and the faster convergence.

Take $\beta_1 = 1$ and $\lambda = 1, 5, 10$, respectively, and the corresponding simulation results are depicted in Figs. 7–11. Specifically, Fig. 7 plots the response curves of the output voltage under the SOSM controller (26) with $\beta_1 = 1$ and different λ, Fig. 8 depicts the response curves of the sliding variable s under different λ, and Figs. 9–11 indicate the response curves of the control signals under different parameters. From Fig. 7, it can be seen that the convergence property improves when λ decreases. Meanwhile, Figs. 9–11 reveal that the smaller λ means the higher frequency of the control signals.

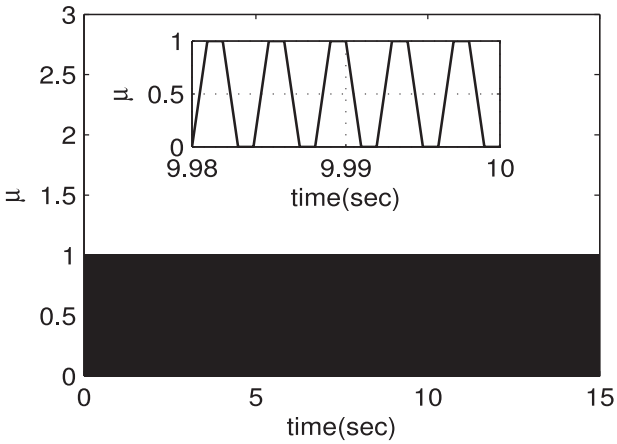

Fig. 11. Response curve of the control signal μ under $\beta_1 = 10, \lambda = 10$.

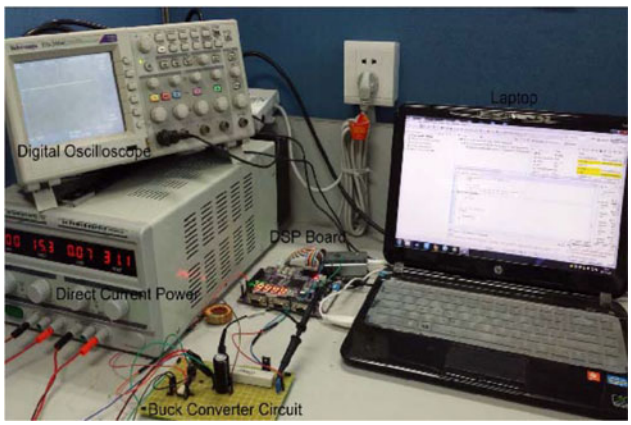

Fig. 12. Experimental test setup.

B. Experimental Results

To evaluate the performance of the proposed method, an experimental platform for the voltage regulation of a buck converter has been built. The specifications of the buck converter are the same as in Table I. The experimental test setup is shown in Fig. 12. The whole SOSM algorithm has been implemented by DSP TMS320F28335 with a clock frequency of 150 MHz. The control algorithm is implemented using a C-program. Two high-precision resistors are connected in parallel for voltage division. The inductance current is measured by the ACS712 current module. The analog signals of output voltage and inductance current are converted to digital signals through two 12-b A/D converters whose sampling period is 40 μs. Then, the square wave signal output from the DSP can be considered as the input of the IR2110 bootstrap chip to control the switch state. The control switch device adopts the IRF630. The detailed configuration of implementation strategy is shown in Fig. 13.

It should be noted that PID controller (28) only uses the voltage signal $v_0(t)$, while the FOSM controller (27) and the SOSM controller (26) utilize both the voltage and current signals. To obtain a good tradeoff between tracking and disturbance rejection performances, we choose the parameters of the PID controller (28) and the FOSM controller (27) as

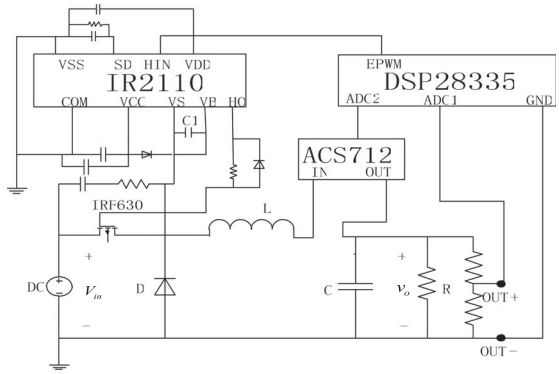

Fig. 13. Configuration of the experimental platform.

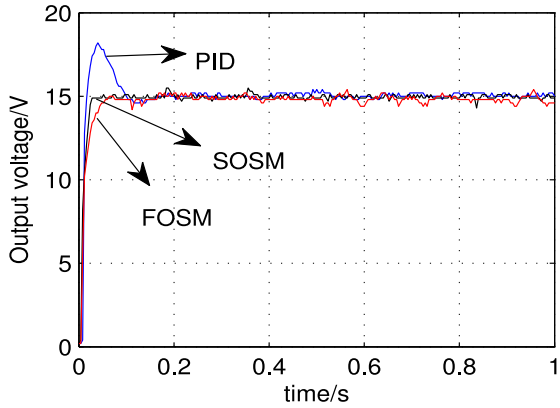

Fig. 14. Experimental start-up transient results of the output voltage v_0 under the PID controller (28), the FOSM controller (27), and the SOSM controller (26) with $\lambda = 1$ and $\beta_1 = 10$.

$K_p = 10, K_i = 5, K_d = 0.1$ and $c_1 = 3, \eta = 200\,000$, respectively. The signum function in FOSM (27) is also replaced by a hysteresis modulation, and the hysteresis width is chosen as $\lambda = 1$.

Fig. 14 shows the experimental start-up results of the output voltage v_0 under the FOSM controller (27), the SOSM controller (26) ($\lambda = 1$ and $\beta_1 = 10$), and the PID controller (28). It can be seen that the SOSM controller (26) obtains the fastest convergence, the FOSM controller (27) comes the second, and the PID controller (28) has the worst convergence. The convergence under the SOSM controller is more rapid than that under the FOSM controller, perhaps because there is no "reaching phase" in SOSM. In addition, no matter how we tune the parameters of the PID controller (28), there is always a small overshoot, while this phenomenon does not occur in the SOSM controller (26) and the FOSM controller (27). This indicates that the start-up performances under the SOSM controller (26) and the FOSM controller (27) are better than that under the PID controller (28).

Fig. 15 shows the experimental start-up results of the output voltage v_0 under the SOSM controller (26) ($\lambda = 1$ and $\beta_1 = 1, 5, 10$). It can be clearly observed that the larger β_1 brings about the faster dynamic performance. In fact, the sliding variable will first converge to the region $\{|\lceil \dot{s} \rfloor|^2 + \beta_1 s| < \lambda\}$, which is similar to the boundary layer in the conventional sliding mode.

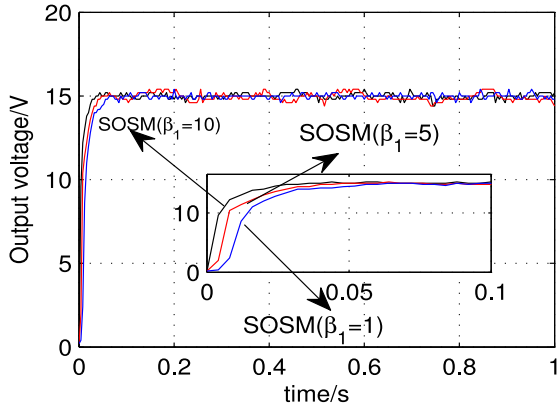

Fig. 15. Experimental start-up transient results of the output voltage v_0 under the SOSM controller (26) with $\lambda = 1$ and $\beta_1 = 1, 5, 10$.

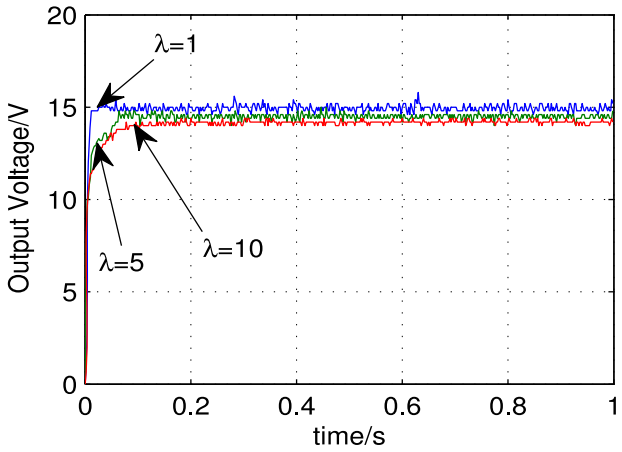

Fig. 16. Experimental start-up transient results of the output voltage v_0 under the SOSM controller (26) with $\beta_1 = 10$ and $\lambda = 1, 5, 10$.

Apparently, the larger β_1 ensures the faster convergence of the sliding variable s. This implies that the experimental results well matched the theoretical analysis.

Now, Fig. 16 depicts the experimental start-up results of the output voltage v_0 under the SOSM controller (26) with different choices of λ. From Fig. 16, we can observe that the smaller λ obtains the faster dynamic performance. It is also seen that if we take $\lambda = 1$, then the output voltage is about 15 V. If λ increases to $\lambda = 5$ ($\lambda = 10$), then the output voltage decreases to about 14 V (13 V). In other words, the smaller λ implies the closer to the desired reference voltage (i.e., 15 V). It can be concluded from Figs. 15 and 16 that the bigger β_1 the faster convergence speed, and the smaller λ the smaller steady-state error.

In what follows, we examine the disturbance rejection properties of the PID controller (28), the FOSM controller (27), and the SOSM controller (26) under different β_1 and λ when load or input voltage changes. The load changes from 50 to 100 Ω, and then back to 50 Ω. The input voltage changes from 30 to 20 V, and then back to 30 V. Fig. 17 shows the output voltage v_0 under the PID controller (28), the FOSM controller (27), and the SOSM controller (26) with $\lambda = 1$ and $\beta_1 = 10$ when the load changes. Fig. 18 gives the disturbance rejection comparisons

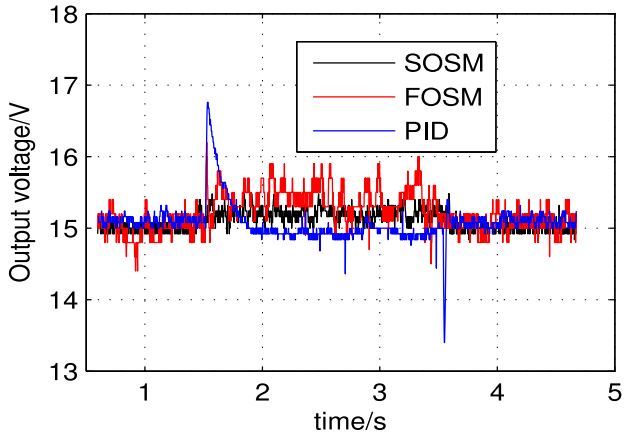

Fig. 17. Experimental step-load transient results of the output voltage v_0 under the PID controller (28), the FOSM controller (27), and the SOSM controller (26) with $\lambda = 1$ and $\beta_1 = 10$.

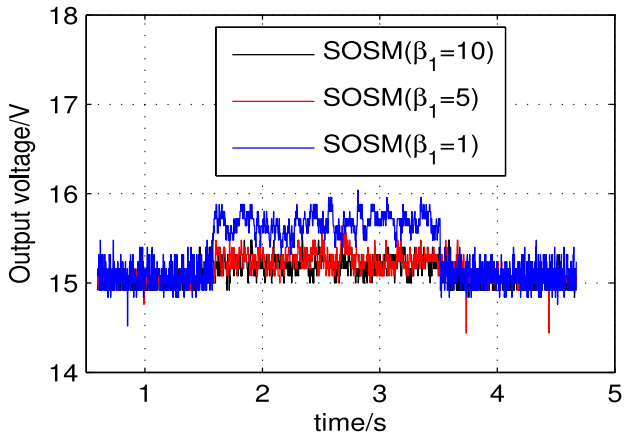

Fig. 18. Experimental step-load transient results of the output voltage v_0 under the SOSM controller (26) with $\lambda = 1$ and $\beta_1 = 1, 5, 10$.

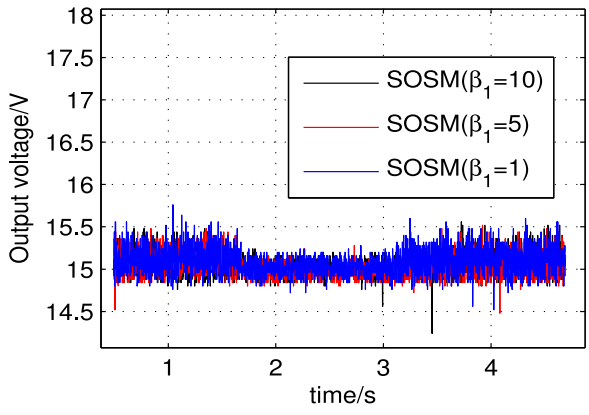

Fig. 19. Experimental step-input-voltage transient results of the output voltage v_0 under the SOSM controller (26) with $\lambda = 1$ and $\beta_1 = 1, 5, 10$.

under the SOSM controller with different β_1 s and the same λ when the load changes. Fig. 19 plots the output voltage v_0 under the SOSM controller (26) with different β_1 and the same λ when the input voltage changes. Fig. 20 displays the output voltage v_0 under the SOSM controller with different λ and $\beta_1 = 10$ when the load changes. Table II gives the maximum output

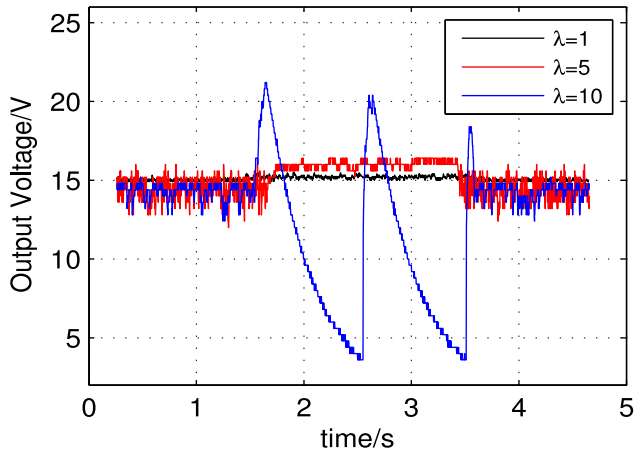

Fig. 20. Experimental step-load transient results of the output voltage v_0 under the SOSM controller (26) with $\beta_1 = 10$ and $\lambda = 1, 5, 10$ when load changes.

TABLE II
COMPARISONS UNDER DIFFERENT β_1 WHEN LOAD CHANGES

Parameters	MOVR/D	MAE
PID	1.76 V	0.1418
$\beta_1 = 1, \lambda = 1$	1.04 V	0.3814
$\beta_1 = 5, \lambda = 1$	0.64 V	0.1613
$\beta_1 = 10, \lambda = 1$	0.48 V	0.1285

TABLE III
COMPARISONS UNDER DIFFERENT λ WHEN LOAD CHANGES

Parameters	MOVR/D	MAE
$\lambda = 1, \beta_1 = 10$	0.48 V	0.1285
$\lambda = 5, \beta_1 = 10$	1.4 V	0.8420
$\lambda = 10, \beta_1 = 10$	11.4 V	3.2096

voltage raise/drop (MOVR/D) and mean absolute error (MAE) comparisons under different β_1, while Table III shows the MOVR/D and MAE comparisons under different λ.

From Fig. 17, it can be observed that both the FOSM controller and the SOSM controller provide the better disturbance rejection property than the PID controller. Fig. 18 shows that under the same λ, the larger β_1 in the SOSM controller (26) provides the better disturbance rejection property. When the input voltage changes from 30 to 20 V, Fig. 19 indicates that the performance under the SOSM controller varies slightly. This phenomenon may be brought on by the large steady-state error of SOSM control. As a matter of fact, the steady-state error in Fig. 19 is caused by the hysteresis bandwidth. This is because there is a contradiction between the hysteresis bandwidth and the control accuracy. The hysteresis bandwidth must be large to reduce chattering; conversely, it should be small to achieve a good control accuracy. In fact, how to reduce the steady-state error is always an important issue for implementation of SMC. An alternative way to reduce the steady-state error in the future may be to use the method given in [29], where the discontinuous element can be smoothed by using a low-pass filter based on the equivalent control method.

Meanwhile, it can also be clearly seen that under the input-voltage variation, there are some differences between the simulation (see Fig. 6) and the experiment (see Fig. 19). From Fig. 19, it is observed that the steady-state error under $\beta_1 = 10$ is smaller than those under $\beta_1 = 5$ and $\beta_1 = 1$, while the steady-state errors under $\beta_1 = 1$ and $\beta_1 = 5$ are similar. This implies that the experimental comparisons under input-voltage variation in Fig. 19 are not that obvious like the simulation comparisons in Fig. 6, because there is a larger steady-state error in the experiment while the steady-state error in the simulation is very small.

Table II also shows us that under the same λ, the bigger β_1 will provide the better disturbance rejection property. This implies that the tuning of the parameter β_1 will not only affect the convergence speed, but also improve the disturbance rejection. Meanwhile, it can be clearly seen from Fig. 20 that the smaller λ of the SOSM controller leads to the better disturbance rejection property. However, Fig. 20 also shows that the larger λ yields the worse steady-state error and even instability, which is also reflected in Table III.

V. CONCLUSION

An SOSM control method has been developed for dealing with the regulation problem of a buck converter in this paper. First, an error variable of freedom of degree 2 can be directly considered as the sliding variable, and thus, the control task can be simplified to the one of designing the controller stabilizing the sliding variable. Second, the finite-time Lyapunov stability for the sliding variables has been tested, while only convergence can be guaranteed in the conventional SMC. Third, the proposed controller has a simple structure and is easy to be implemented. The feasibility and effectiveness of the proposed SOSM controller have been demonstrated by experimental studies. Our future work will focus on dc–dc buck converters with more power to further test the robustness performances of SOSM algorithms.

REFERENCES

[1] C. Chen *et al.*, "Online inductor parameters identification by small signal injection for sensorless predictive current controlled boost converter," *IEEE Trans. Ind. Informat.*, vol. 13, no. 4, pp. 1554–1564, Aug. 2017.

[2] B. Amir and M. Dragan, "Hybrid digital adaptive control for fast transient response in synchronous buck DC-DC converters," *IEEE Trans. Power Electron.*, vol. 24, no. 11, pp. 2625–2638, Nov. 2009.

[3] D. Maria, P. Marcello, and R. Antoella, "Analytical versus neural real-time simulation of a photovoltaic generator based on a DC-DC converter," *IEEE Trans. Ind. Appl.*, vol. 46, no. 6, pp. 2501–2510, Nov./Dec. 2010.

[4] C. L. Zhang, J. X. Wang, S. H. Li, B. Wu, and C. Qian, "Robust control for PWM-based DC-DC buck power converters with uncertainty via sampled-data output feedback," *IEEE Trans. Power Electron.*, vol. 30, no. 1, pp. 504–515, Jan. 2015.

[5] R. Silva-Ortigoza, V. Hernndez-Guzmn, M. Antonio-Cruz, and D. Muoz-Carrillo, "DC/DC buck power converter as a smooth starter for a DC motor based on a hierarchical control," *IEEE Trans. Power Electron.*, vol. 30, no. 2, pp. 1076–1084, Feb. 2015.

[6] S. Biricik and H. Komurcugil, "Optimized sliding mode control to maximize existence region for single-phase dynamic voltage restorers," *IEEE Trans. Ind. Informat.*, vol. 12, no. 4, pp. 1486–1497, Aug. 2016.
[7] C. S. Chiu and C. T. Shen, "Finite-time control of DC-DC buck converters via integral terminal sliding modes," *Int. J. Electron.*, vol. 99, no. 5, pp. 643–655, 2012.
[8] Y. Ni and J. P. Xu, "Optimal design of sliding mode control buck converter with bounded input," *ACTA Electron. Sinica*, vol. 41, no. 3, pp. 555–560, 2013.
[9] Y. Huangfu, R. Ma, E. Xie, and M. Abdellatif, "A robust second order sliding mode controller for buck converter," in *Proc. Int. Conf. Elect. Mach. Syst.*, Incheon, South Korea, Dec. 2010, pp. 159–161.
[10] S. C. Tan, Y. M. Lai, M. K. H. Cheung, and C. K. Tse, "On the practical design of a sliding mode voltage controlled buck converters," *IEEE Trans. Power Electron.*, vol. 20, no. 2, pp. 425–437, Mar. 2005.
[11] E. C. Chang, T. J. Liang, J. F. Chen, and F. J. Chang, "Real-time implementation of grey fuzzy terminal sliding mode control for PWM DC-AC converters," *IET Power Electron.*, vol. 1, no. 2, pp. 235–244, 2008.
[12] H. Komurcugil, "Non-singular terminal sliding-mode control of DC-DC buck converters," *Control Eng. Pract.*, vol. 21, no. 3, pp. 321–332, 2013.
[13] S. He, J Song, and F. Liu, "Robust finite-time bounded controller design of time-delay conic nonlinear systems using sliding mode control strategy," *IEEE Trans. Syst. Man Cybern., Syst.*, 2017, doi: 10.1109/TSMC.2017.2695483, to be published.
[14] S. H. Ding, L. Liu, and W. X. Zheng, "Sliding mode direct yaw-moment control design for in-wheel electric vehicles," *IEEE Trans. Ind. Electron.* vol. 64, no. 8, pp. 6752–6762, Aug. 2017.
[15] H. Baghaee, M. Mirsalim, G. Gharehpetian, and H. Talebi, "A decentralized power management and sliding mode control strategy for hybrid AC/DC microgrids including renewable energy resources," *IEEE Trans. Ind. Informat.*, 2017, doi: 10.1109/TII.2017.2677943, to be published.
[16] R. Ling, D. Maksimovic, and R. Leyva, "State-machine realization of second-order sliding-mode control for synchronous buck DC-DC converters," in *Proc. 5th IEEE Energy Convers. Congr. Expo.*, Denver, CO, USA, Sep. 2013, pp. 125–133.
[17] R. Ling, D. Maksimovic, and R. Leyva, "Second-order sliding-mode controlled synchronous buck DC-DC converter," *IEEE Trans. Power Electron.*, vol. 31, no. 3, pp. 2539–2549, Mar. 2016.
[18] C. Qian and W. Lin, "A continuous feedback approach to global strong stabilization of nonlinear systems," *IEEE Trans. Automat. Control*, vol. 46, no. 7, pp. 1061–1079, Jul. 2001.
[19] S. H. Ding, A. Levant, and S. H. Li, "Simple homogeneous sliding-mode controller," *Automatica*, vol. 67, pp. 22–32, 2016.
[20] S. C. Tan, Y. M. Lai, and C. K. Tse, *Sliding Mode Control of Switching Power Converters*. New York, NY, USA: CRC Press, 2012.
[21] S. H. Ding and S. H. Li, "Second-order sliding mode controller design subject to mismatched term," *Automatica*, vol. 77, pp. 388–392, 2017.
[22] G. H. Hardy, J. E. Littlewood, and G. Polya, *Inequalities*. Cambridge, U.K.: Cambridge Univ. Press, 1952.
[23] A. Levant, "Sliding order and sliding accuracy in sliding mode control," *Int. J. Control*, vol. 58, no. 6, pp. 1247–1263, 1993.
[24] G. Bartolini, A. Pisano, E. Punta, and E. Usai, "A survey of applications of second-order sliding mode control to mechanical systems," *Int. J. Control*, vol. 76, no. 9–10, pp. 875–892, 2003.
[25] S. P. Bhat and D. S. Bernstein, "Finite-time stability of continuous autonomous system," *SIAM J. Control Optim.*, vol. 38, no. 3, pp. 751–766, 2000.
[26] X. Xie, D. Yue, T. Ma, and X. Zhu, "Further studies on control synthesis of discrete-time T-S fuzzy systems via augmented multi-indexed matrix approach," *IEEE Trans. Cybern.*, vol. 44, no. 12, pp. 2784–2791, Dec. 2014.
[27] S. C. Tan, Y. M. Lai, and K. H. Cheung, "A fixed-frequency pulse width modulation based quasi-sliding-mode controller for buck converters," *IEEE Trans. Power Electron.*, vol. 20, no. 6, pp. 1379–1392, Nov. 2005.
[28] S. H. Ding, J. D. Wang, and W. X. Zheng, "Second-order sliding mode control for nonlinear uncertain systems bounded by positive functions," *IEEE Trans. Ind. Electron.*, vol. 62, no. 9, pp. 5899–5909, Sep. 2015.
[29] V. Utkin and J. Shi, "Integral sliding mode in systems operating under uncertainty conditions," in *Proc. 35th IEEE Conf. Decision Control*, Kobe, Japan, 1996, pp. 4591–4596.

Shihong Ding (M'12) was born in Ma An Shang, Anhui, China, in 1983. He received the B.E. degree in mathematics from Anhui Normal University, Wuhu, China in 2004, and the M.S. and Ph.D. degrees in automatic control from Southeast University, Nanjing, China, in 2007 and 2010, respectively.

During his graduate studies, he visited the University of Texas at San Antonio from August 2008 to August 2009. After graduation, he held a research fellowship at the University of Western Sydney for one year. He is currently a Professor with the School of Electrical and Information Engineering, Jiangsu University, Zhenjiang, China. His research interests include sliding-mode control and vehicle dynamics.

Wei Xing Zheng (M'93–SM'98–F'14) received the Ph.D. degree in electrical engineering from Southeast University, Nanjing, China in 1989.

Over the years, he has held various faculty/research/visiting positions at Southeast University, Nanjing, China; the Imperial College of Science, Technology and Medicine, London, U.K.; the University of Western Australia, Perth, Australia; the Curtin University of Technology, Perth, Australia; the Munich University of Technology, Munich, Germany; the University of Virginia, Charlottesville, VA, USA; and the University of California at Davis, Davis, CA, USA. He is currently a Full Professor with Western Sydney University, Sydney, Australia.

Dr. Zheng is a Fellow of IEEE and was named as a Thomson Reuters Highly Cited Researcher in 2015, 2016 and 2017 consecutively. Previously, he served as an Associate Editor for the IEEE TRANSACTIONS ON CIRCUITS AND SYSTEMS—PART I: FUNDAMENTAL THEORY AND APPLICATIONS, the IEEE TRANSACTIONS ON AUTOMATIC CONTROL, IEEE SIGNAL PROCESSING LETTERS, the IEEE TRANSACTIONS ON CIRCUITS AND SYSTEMS—PART II: EXPRESS BRIEFS, and the IEEE TRANSACTIONS ON FUZZY SYSTEMS, and as a Guest Editor for the IEEE TRANSACTIONS ON CIRCUITS AND SYSTEMS—PART I: REGULAR PAPERS. He is currently an Associate Editor for *Automatica*, the IEEE TRANSACTIONS ON AUTOMATIC CONTROL (the second term), the IEEE TRANSACTIONS ON CYBERNETICS, the IEEE TRANSACTIONS ON NEURAL NETWORKS AND LEARNING SYSTEMS, the IEEE TRANSACTIONS ON CONTROL OF NETWORK SYSTEMS, and other scholarly journals. He has also served as the Chair of IEEE Circuits and Systems Society's Technical Committee on Neural Systems and Applications and as the Chair of IEEE Circuits and Systems Society's Technical Committee on Blind Signal Processing.

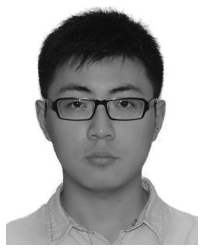

Jinlin Sun was born in Yangzhou, Jiangsu, China, in 1994. He received B.E. degree in automatic control from Jiangsu University, Zhenjiang, China, in 2016. He is currently working toward the Ph.D. degree with the Institute of Automation, Chinese Academy of Sciences, Beijing, China.

His current research interests include sliding-mode control and computational intelligence.

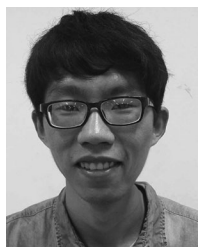

Jiadian Wang was born in Nantong, China, in 1990. He received the B.S. degree in automation from Jiangsu University of Science and Technology, Zhenjiang, China, in 2013. In 2016, he received the Master degree in automatic control from Jiangsu University, Zhenjiang, China.

His current research interests include sliding-mode control and DC–DC converters.